ELSEVIER

Journal of Chromatography A, 971 (2002) 105–116

JOURNAL OF CHROMATOGRAPHY A

www.elsevier.com/locate/chroma

Protein adsorption on novel acrylamido-based polymeric ion-exchangers
IV. Effects of protein size on adsorption capacity and rate

Alan K. Hunter, Giorgio Carta*

Department of Chemical Engineering, University of Virginia, PO Box 400741, Charlottesville, VA 22903-2442, USA

Received 7 February 2002; received in revised form 5 July 2002; accepted 5 July 2002

Abstract

The effects of protein size on the adsorption capacity and rate is determined for an acrylamido-based polymeric anion-exchanger. The proteins lactalbumin, myoglobin, ovalbumin, BSA, conalbumin, IgG, and ferritin with molecular masses ranging from 15 000 to 450 000 were investigated. At high salt concentration (50 m*M* Tris–HCl containing 500 m*M* NaCl), only the smaller proteins lactalbumin and myoglobin gained access to a significant portion of the particle volume. The larger proteins were nearly completely excluded, in agreement with the results obtained for neutral macromolecules. By contrast, at low salt concentration (50 m*M* Tris–HCl), the adsorption capacity was very large (280–400 mg/ml of particle volume) for all the proteins studied except for ferritin, for which the capacity was much lower. This suggests that, provided the solute is not too large, the favorable electrostatic interaction overcomes the size exclusion effect. Adsorption rate measurements showed that mass transfer rates are also quite fast at low salt concentration. Effective diffusivities were determined by matching model and experimental results and were found to decrease substantially as the protein size increased. As previously observed, the homogeneous diffusion model was found to predict the experimentally observed trends with respect to protein concentration and boundary layer mass transfer effects.

Keywords: Polymeric gels; Mass transfer; Stationary phases, LC; Proteins

1. Introduction

Ion exchange media are used extensively for the process-scale separation of proteins, especially in capture applications [1]. Both the equilibrium uptake capacity and the rate of mass transfer affect the performance of ion-exchangers in these applications. Thus, an understanding of how these properties are influenced by protein size is needed. Mass transfer within the adsorbent particle is especially important since it is typically the principal cause of band broadening [2].

Many previous studies have investigated protein mass transfer in ion-exchangers. However, most of these studies have considered a single protein on one stationary phase [3–5] or one protein on different stationary phases [6–11]. A number of authors have investigated the mass transport properties of different proteins on the same stationary phase under linear or non-binding conditions at high salt concentrations

*Corresponding author. Tel.: +1-434-924-6281; fax: +1-434-982-2658.

E-mail address: gc@virginia.edu (G. Carta).

0021-9673/02/$ – see front matter
PII: S0021-9673(02)01027-0

[12–16]. However, it has been shown that transport rates in ion-exchangers often vary with ionic strength [8,10,17,18] so that kinetic parameters obtained for these conditions may not be representative of the rates obtained for overloaded conditions at low salt concentrations.

Only a few authors have reported systematic rate measurements for a range of differently sized proteins under strong binding conditions. Skidmore et al. [19] examined the adsorption of lysozyme and BSA on S-Sepharose-FF. They fit experimental uptake data using a pore diffusion model and found that the ratio of effective pore diffusivity and the free solution diffusivity was substantially smaller for BSA than for lysozyme. This was attributed to the diffusion of BSA being restricted to a greater extent than that of lysozyme. Garke et al. [20] investigated batch uptake of lysozyme and γ-globulin on Streamline SP, a macroporous agarose resin. The ratio of effective pore and free solution diffusivities were 0.20 and 0.38 for lysozyme and γ-globulin, respectively. However, these ratios decreased at higher protein concentrations and this effect was attributed to increased interactions with the pore walls. Johnston and Hearn [21] investigated the adsorption of human serum albumin, carbonic anhydrase, and ferritin on a number of macroporous weak anion-exchangers. Their findings suggest that the effective pore diffusivity of the smaller proteins was close to the free solution diffusivity, indicating negligible restriction to mass transfer through the pores. However, the effective pore diffusivity of ferritin was found to be only 1/40 of that in free solution, consistent with severely hindered diffusion. Lewus and Carta [22] investigated the uptake of lysozyme and cytochrome-*c* on S-HyperD-M, which is composed of a porous silica matrix filled with a functionalized polyacrylamide gel. The single component kinetics of these two similarly sized proteins was similar and both yielded effective pore diffusivities higher than the corresponding free solution diffusivities. Fernandez and Carta [23] studied the batch uptake of α-lactalbumin, ovalbumin, and BSA on Q-HyperD. While BSA was observed to have the lowest intraparticle diffusivity, the diffusivities of α-lactalbumin and ovalbumin were found to be very similar, despite the fact that ovalbumin is substantially larger. In all three cases, the effective pore diffusivities were larger than the corresponding solution diffusivities.

Recently, we have described the adsorptive properties of a new acrylamido-based anion-exchanger known as BRX-Q (BioRad) [18,24,25]. This material showed a very high equilibrium adsorption capacity for BSA, high mass transfer rates, and a very high dynamic binding capacity. These high-performance characteristics were attributed to its unique structure, which was shown to comprise a low-density gel interspersed within a denser polymeric phase. Thus, qualitatively, BRX-Q has some of characteristics of Q-HyperD, namely high capacity and rapid diffusion. However, BRX-Q is made in a single step while Q-HyperD is a composite based on a gel contained in a silica support matrix. The chemical nature of the polymer in BRX-Q is also different since it is based on a mixture of acrylamido and vinylic monomers. In this work we extend our measurements of equilibrium uptake and mass transfer rates to a broad set of representative proteins with molecular masses ranging between 15 000 and 450 000.

2. Materials and methods

2.1. Materials

BRX-Q samples were obtained from Bio-Rad (Hercules, CA, USA). This material is a strong anion-exchanger based on water-soluble, acrylamido and vinylic monomers polymerized to yield spherical particles. The anion-exchange functionality derives from the use of a monomer possessing a quaternary ammonium ion group. Thus, no post-polymerization derivatization is necessary since the ionogenic monomer is incorporated directly in the final product. A version of BRX-Q with substantially similar structure and properties has recently become available commercially from Bio-Rad and is marketed under the trade name UNOSphere Q. The physical properties of BRX-Q, including particle size distribution, apparent and skeletal densities, ion-exchange capacity, scanning electron microscopy of dried beads, and transmission electron microscopy of thin sections of resin-embedded beads, are given in Ref. [24]. This material was shown to possess a heterogeneous structure. The mean particle diameter for the material

used in this work is 89 μm. The samples were washed in a gravity-fed column with alternating cycles of 500 m*M* NaCl and dilute buffer solutions and stored under refrigeration in buffer.

All of the proteins used in this study were obtained from Sigma (St. Louis, MO, USA) except IgG that was from Pharmacia & Upjohn (Kalamazoo, MI, USA). Table 1 summarizes molecular masses, isoelectric points, free solution diffusivities, and radii of the proteins used. The p*I* values given are typical values reported in the literature, as indicated, but it should be recognized that significant variations could occur depending on the source of the protein. Similarly, the solution diffusivity values represent experimental or estimate averages. Finally, the radius of gyration calculated from diffusivities merely represents the spatial requirements for diffusion in solution [27] and may be different from the actual size of the protein, especially for the less spherical proteins such as BSA and IgG. Dextran T-500 was obtained from Amersham Pharmacia Biotech (Piscataway, NJ, USA). Other chemicals were obtained from Sigma and from Fisher Scientific (Pittsburgh, PA, USA). All experiments were conducted at room temperature (22±2 °C) in a 50-m*M* Tris–HCl buffer. The pH was 9.5 for experiments with conalbumin, and 8.5 for all the other proteins.

Table 1
Properties of the proteins used in this work

Protein	M_r	pI[a]	D_0[b] (10^7 cm^2/s)	R_g[c] (nm)
Lactalbumin	15 000	5.1	10.6	1.6
Myoglobin	17 000	7.0	11.3	1.5
Ovalbumin	45 000	4.7	7.4	2.3
BSA	66 500	4.9	6.0	2.8
Conalbumin	80 000	6.2	5.7	3.0
IgG	160 000	6.5	3.9	4.3
Ferritin	450 000	4.4	3.6	5.0

[a] Typical values from Refs. [16,20,26].
[b] Average of experimental values in Ref. [27], except for lactalbumin from Ref. [16], and conalbumin from the correlation of Young et al. [28].
[c] Radius of gyration from diffusion data obtained from Eq. (8) in Ref. [27].

2.2. Methods

2.2.1. Adsorption isotherms

Adsorption isotherms were obtained by placing small samples of hydrated media (~0.025 g) in vials with a volume (6 ml) of a solution containing a known initial protein concentration, C_0. The vials were sealed and rotated end-to-end at a few rpm and the supernatant analyzed for protein content with a UV spectrophotometer (Beckman Coulter, Fullerton, CA, USA; Model DU-50). The uptake of protein by the media was calculated from a material balance. Equilibrium was established in 12 h or less as shown by the absence of any further changes in protein concentration in the supernatant.

2.2.2. Chromatography

Isocratic elution experiments were conducted using dextran T-500, glucose, lactalbumin, ovalbumin, BSA, and conalbumin in a 50 m*M* Tris–HCl buffer at pH 8.5 containing 500 m*M* NaCl. Myoglobin (M_r = 17 000, pI = 7.0) was also used in these experiments. BRX-Q was flow packed at 8 ml/min in a 1-cm I.D. glass column (Pharmacia, Model HR 10/10) to a bed height of 10 cm and operated at 1 ml/min (76 cm/h) with a Pharmacia Model P-500 syringe pump. Protein and dextran samples in buffer (0.05 ml, 2.0–2.5 mg/ml) were injected with a Rheodyne six-port valve. A Waters (Milford, MA, USA) Model 484 UV–Vis detector at 280 nm was used for the proteins, while a Waters Model R401 differential refractive index detector was used for dextran T-500 and glucose. Corrections were made as described in Hunter and Carta [24] to account for the extra column volume.

2.2.3. Stirred-batch experiments

Uptake rates were measured in an agitated contactor at initial protein concentrations of 0.2, 1, and 2 mg/ml. The experimental apparatus used is described in Refs. [11,23]. The volume of the protein solution used was 100 ml and the amount of media was adjusted for each protein to yield a final solution concentration of 0.5 mg/ml when using an initial protein concentration of 1 mg/ml. The solution was stirred magnetically at ~300 rpm and the protein concentration was obtained by circulating a stream through a UV spectrophotometer at 280 nm. Microscopic observation of the beads after stirring showed that no visible damage occurred, which was expected

since the vessel used is designed for cell culture and, hence, to minimize mechanical wear to suspended particles.

3. Results and discussion

3.1. Adsorption isotherms

The equilibrium uptake isotherms are shown in Fig. 1. The isotherms are all highly nonlinear. With the exception of ferritin, for which the capacity is very low, maximum uptake capacities are in the range 280–400 mg/ml. Within this range, although the correlation between uptake capacity and molecular mass is not exact, the capacity is generally smaller for the larger proteins. For ferritin the uptake capacity is very small presumably because its size exceeds what can be accommodated by the particle structure.

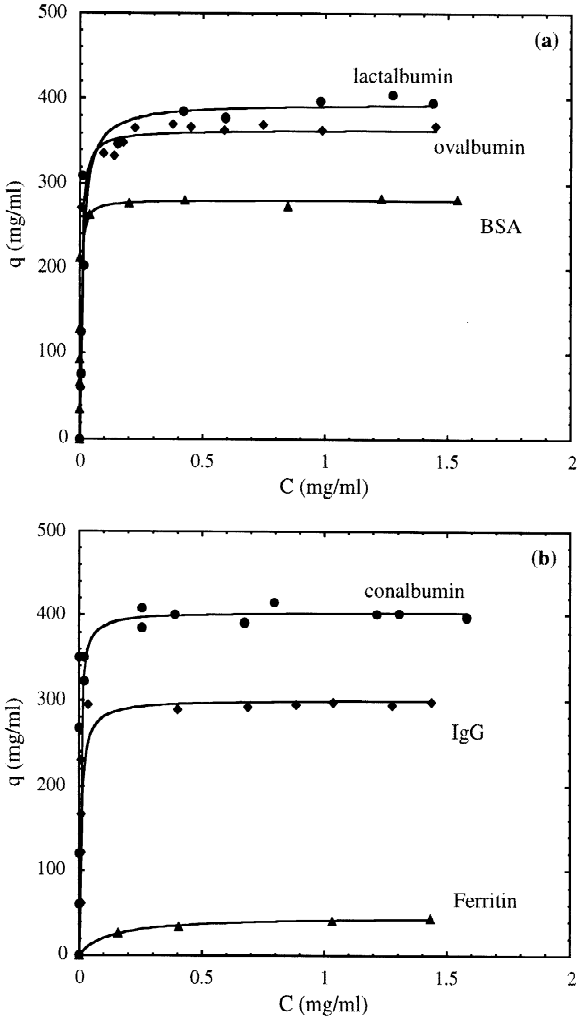

Fig. 1. Adsorption isotherms for BRX-Q in 50 m*M* Tris–HCl buffer: (a) lactalbumin, ovalbumin, and BSA and (b) conalbumin, IgG, and ferritin.

The solid lines in Fig. 1 represent Langmuir isotherms calculated from:

$$q = \frac{q_m bC}{1 + bC} \quad (1)$$

where q_m and b are fitted parameters. Their values are summarized in Table 2. As has been shown previously, BRX-Q is composed of dense polymer aggregates interspersed in a charged gel phase [24]. The dense aggregates provide structural strength while the surrounding gel provides adsorption capacity. Prior SEC experiments using neutral macromolecules have shown that the size exclusion limit of BRX-Q is very low, with gel pores approximately 0.6–2 nm [24]. Thus, under binding conditions the favorable electrostatic interaction between the protein and the stationary phase has to overcome the unfavorable size exclusion interaction. For larger proteins, the barrier imposed by size may be to great to overcome, as is apparently the case for ferritin.

3.2. Chromatography under non-binding conditions

The results of elution chromatography experiments for different proteins, glucose, and dextran T-500 (M_r~500 000) in Tris–HCl buffer containing 500 m*M* NaCl are shown in Fig. 2. As shown in our prior

Table 2
Equilibrium parameters in 50 m*M* Tris–HCl buffer at pH 8.5

Protein	q_m (mg/ml)	b (ml/mg)
Lactalbumin	390	100
Ovalbumin	360	210
BSA[a]	280	500
Conalbumin[b]	400	250
IgG	300	140
Ferritin	50	5

[a] From Ref. [18].
[b] pH 9.5.

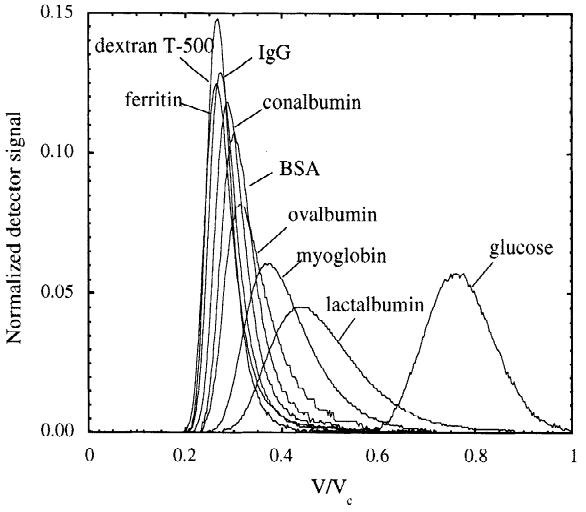

Fig. 2. Chromatography peaks for BRX-Q column for non-binding conditions in 50 m*M* Tris–HCl buffer at pH 8.5 containing 500 m*M* NaCl.

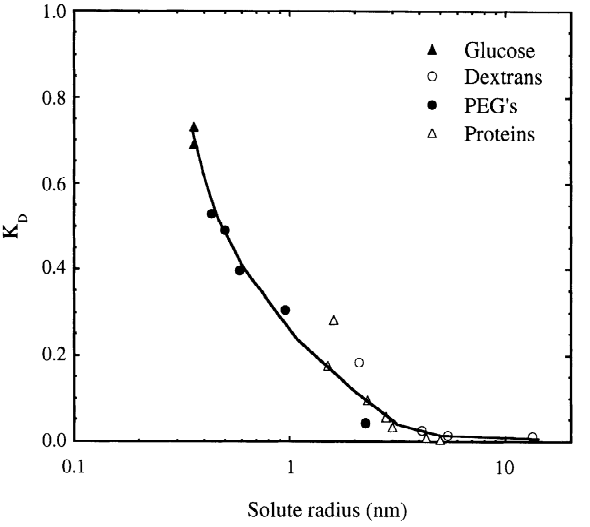

Fig. 3. Distribution coefficients for proteins, PEGs, dextrans, and glucose as a function of solute radius. Proteins and glucose in 50 m*M* Tris–HCl buffer at pH 8.5 containing 500 m*M* NaCl. PEGs and dextran in 50 m*M* Tris–HCl buffer at pH 8.5 data are from Ref. [24].

work [24], the normalized retention volume of dextran T-500 (V_e/V_c~0.3) is close to the extraparticle void fraction, ε_b. At this salt concentration, all of the proteins, except for lactalbumin and myoglobin, elute with retention times very close to dextran T-500. This confirms that when the electrostatic interaction is suppressed at high ionic strength, the larger proteins are almost completely excluded from the intraparticle space. The behavior of the smaller lactalbumin and myoglobin is somewhat different as these proteins gain access to a significant portion of the intraparticle space (V_e/V_c~0.5). Distribution coefficients were calculated according to:

$$K_D = \frac{\frac{V_e}{V_c} - \varepsilon_b}{1 - \varepsilon_b} \quad (2)$$

The elution volume V_e/V_c was obtained from the first moment of the elution peaks. The results are shown in Fig. 3 along with values previously obtained for glucose, PEG, and dextran standards [24] plotted as a function of the solute radius. For glucose, the PEGs, and the dextrans this was calculated as shown in Ref. [24], while for the proteins it was calculated as the radius of gyration from the free solution diffusivity data (see Table 1) [27]. There is a good agreement between values obtained for the neutral probes and those obtained with the proteins at high salt concentration. As shown in Ref. [18], the salt concentration makes little difference with regards to the retention behavior of the neutral probes. Thus, we can conclude that the electrostatic interaction with the media functional groups is shielded, the proteins behave like the correspondingly sized neutral probes. For these conditions, proteins with a radius in the range of 3 nm or larger are thus nearly completely excluded from the media. The largest K_D value is found for lactalbumin. However, this value is still less than one half the value determined for glucose.

HETP values were also calculated for each solute using the tangent method and the results are shown in Table 3 as $h = \mathrm{HETP}/d_p$. Although this is only an approximation because of the relative peak skewness [29], it still provides a useful lower-bound estimate of the actual HETP. For the conditions of our experiments, the HETP is given by:

$$h = a + \frac{1}{30}\frac{\varepsilon_b}{1-\varepsilon_b}\left(\frac{k'}{1+k'}\right)^2\left[\frac{10}{Sh} + \frac{D_0}{D_e}\right] \quad (3)$$

where $k' = (1-\varepsilon_b)K_D/\varepsilon_b$ is the retention factor,

Table 3
Parameters from isocratic elution experiments in 50 m*M* Tris–HCl buffer containing 500 m*M* NaCl

Solute	K_D	h	D_e/D_0
Glucose	0.70	12	0.58
Lactalbumin	0.28	46	0.041
Myoglobin	0.18	35	0.031
Ovalbumin	0.095	25	0.032
BSA	0.057	17	0.038
Conalbumin	0.034	15	0.024
IgG	0.0098	13	0.0065
Ferritin	0.0042	13	0.0013
Dextran T-500	0	11	0

$Sh = k_f d_p/D_0$ is the Sherwood number, D_e is the effective pore diffusivity, and $v' = vd_p/D_0$ is the reduced velocity [30]. Since for our experimental conditions *Sh* is expected to be larger than 10 while D_e/D_0 is expected to be less than unity [30], the term in brackets is dominated by D_e/D_0. Moreover, the *a*-term in Eq. (3), which accounts for axial dispersion, can be estimated from the results for dextran T-500, for which $K_D \sim 0$. It should be noted that, in general, the *a*-term is also affected by the reduced velocity (cf. Knox equation). However, in our case, this effect was likely small since the reduced velocity was high, around 100 for glucose and greater than 570 for the proteins. Thus, the term D_e/D_0 can be estimated from these data. As seen in Table 3, the HETP decreases as the protein size increases. This apparently inconsistent result is due to the fact that the K_D values are very small. As a result, the term $k'/(1+k')$ in Eq. (3) plays a significant role. This term decreases as K_D decreases. The D_e/D_0 ratio is very small (≤ 0.041) for all the proteins studied indicating a large diffusional hindrance under these non-binding conditions. For glucose, on the other hand, this ratio is about 0.58 suggesting that this small molecule encounters little diffusional hindrance. In this case, band spreading is dominated by axial dispersion.

3.3. Adsorption kinetics

Batch uptake curves in 50 m*M* Tris–HCl buffer showing the normalized fluid phase protein concentration, C/C_0, for lactalbumin, ovalbumin, conalbumin, and IgG are given in Fig. 4 and the corresponding protein concentrations in the particle, $\bar{q}$, are given in Fig. 5, both as a function of time. The former was measured directly and the latter was obtained from a material balance. As seen in Fig. 5, the uptake rates are obviously smaller with the larger proteins and, in each case, increase as the initial protein concentration is increased from 0.2 to 1 mg/ml. However, increasing the initial protein concentration further to 2 mg/ml results in only a relatively small increase in the uptake rate. As seen in Fig. 4, the initial portion of the curves showing C/C_0 vs. time obtained with different initial concentrations are coincident for a substantial length of time. This behavior suggests that the external film mass transfer resistance controls the initial rate of adsorption.

The batch uptake of BSA on BRX-Q has previously been shown to be consistent with a homogeneous diffusion model given by the following equations [25]:

$$\frac{\partial q}{\partial t} = \frac{D_s}{r^2}\frac{\partial}{\partial r}\left(r^2\frac{\partial q}{\partial r}\right) \tag{4}$$

$$t = 0,\ q = 0 \tag{4a}$$

$$r = 0,\ \frac{\partial q}{\partial r} = 0 \tag{4b}$$

$$r = r_p,\ q = q_i,\ D_s\frac{\partial q}{\partial r} = k_f(C - C_i) \tag{4c}$$

$$\frac{dC}{dt} = \frac{V_M}{V}\frac{d\bar{q}}{dt} = -\frac{3k_f}{r_p}\frac{V_M}{V}(C - C_i) \tag{5}$$

$$t = 0,\ C = C_0,\ \bar{q} = 0 \tag{5a}$$

where q is the adsorbed protein concentration, D_s is the effective diffusivity, r_p is the particle radius, k_f is the external film mass transfer coefficient, C and C_i are the protein concentration in the bulk fluid and the particle surface, and V and V_M are the solution and adsorbent particle volumes, respectively. C_i varies with time and is related to $q(t, r = r_p)$ through the adsorption isotherm, Eq. (1). This model assumes that the intraparticle mass transfer flux is proportional to the gradient in the adsorbed protein concentration in the particle.

A numerical solution is required in general. However, when the isotherm is very favorable, as in our case, the following two asymptotic limits exist [31], dependent on the parameter:

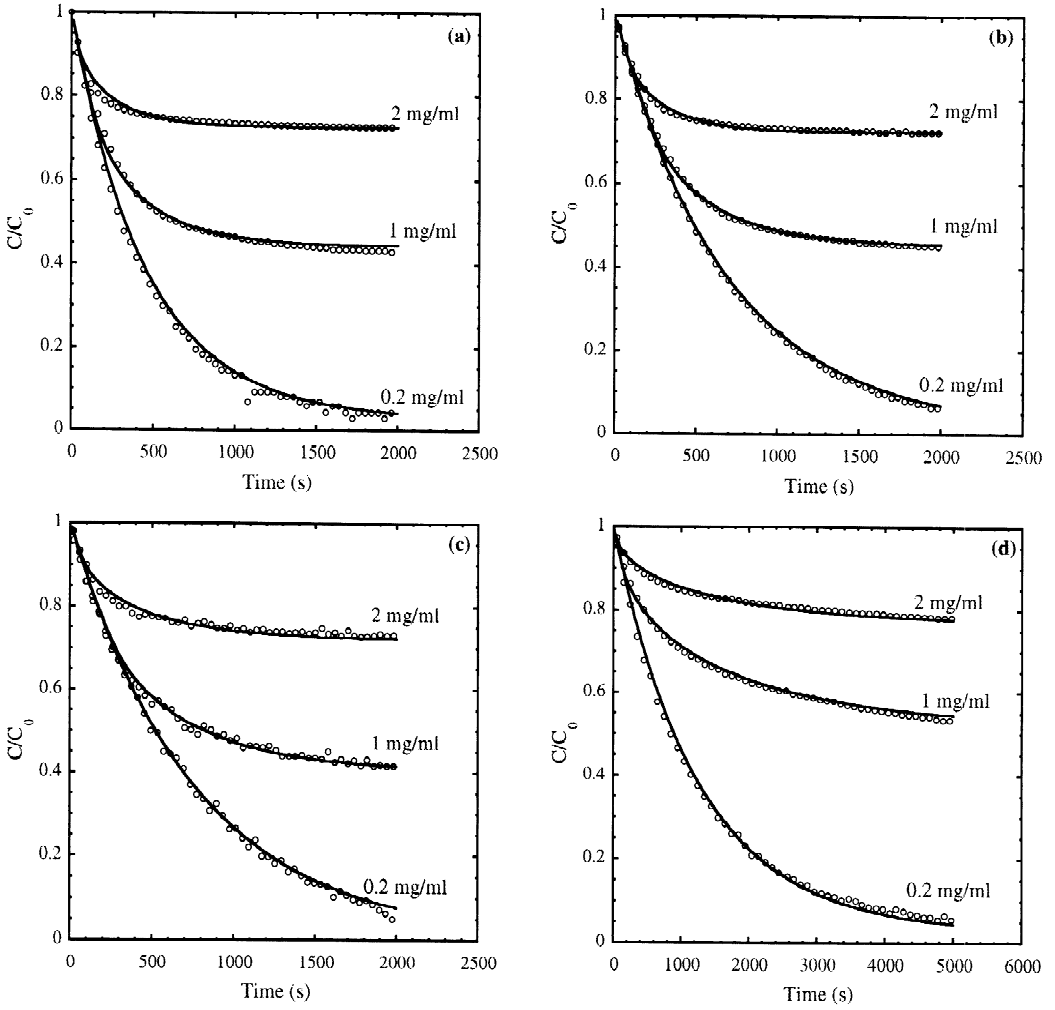

Fig. 4. Batch uptake curves for (a) lactalbumin, (b) ovalbumin, (c) conalbumin, and (d) IgG in 50 m*M* Tris–HCl buffer showing the normalized fluid phase concentration as a function of time for different initial concentrations. Solid lines are calculated with the homogeneous diffusion model with parameters in Tables 2 and 4.

$$\delta = \frac{1}{5}\frac{k_f r_p}{D_s}\frac{C_0}{q_m} \tag{6}$$

When $\delta < 1$, the external film resistance is dominant and the solution is approximated by:

$$\frac{C}{C_0} = \exp\left(-\frac{3k_f}{r_p}\frac{V_M}{V}t\right) \tag{7}$$

Conversely, when $\delta \gg 1$, intraparticle diffusion is completely dominant and the solution is approximated by:

$$\frac{\bar{q}}{q_m} = 1 - \frac{6}{\pi^2}\sum_{n=1}^{\infty}\frac{1}{n^2}\exp\left(-\frac{n^2\pi^2 D_s t}{r_p^2}\right) \tag{8}$$

It can bee seen that these two asymptotic limits are consistent with the experimental trends. For short times and low initial concentrations, the data conform to Eq. (7) with the ratio C/C_0 being independent of C_0. Conversely, at high initial concentrations, the uptake rate exhibits only a small dependence on C_0, consistent with Eq. (8).

The solid lines in Figs. 4 and 5 were obtained from the numerical solution of Eqs. (1), (4) and (5).

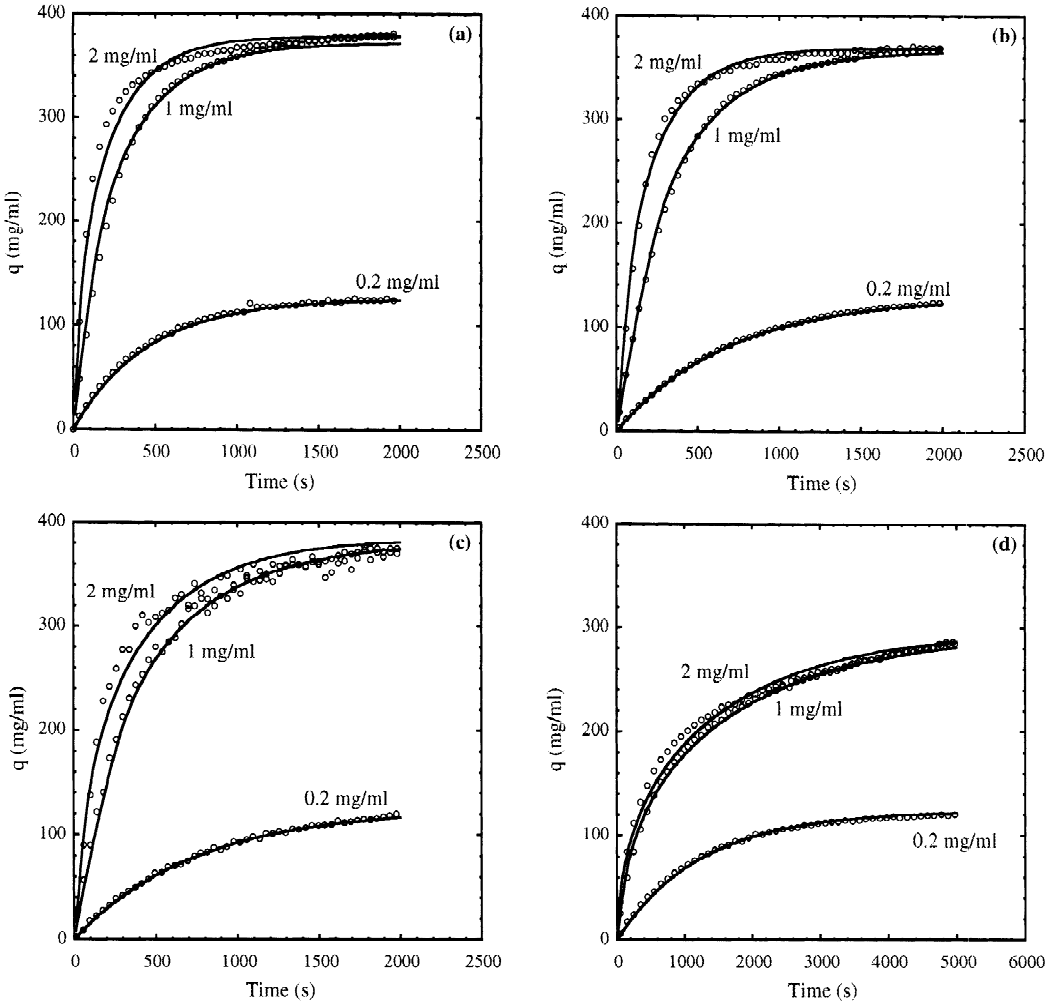

Fig. 5. Batch uptake curves for (a) lactalbumin, (b) ovalbumin, (c) conalbumin, and (d) IgG in 50 m*M* Tris–HCl buffer showing the protein concentration in the adsorbent particles for different initial protein concentrations. Solid lines are calculated with the homogeneous diffusion model with parameters in Tables 2 and 4.

The equations were solved numerically by orthogonal collocation as discussed in Ref. [32] using the equilibrium parameters in Table 2. The film mass transfer coefficient was obtained by fitting Eq. (7) to the uptake data at $C_0 = 0.2$ mg/ml, while the diffusivity was obtained by matching experimental and calculated curves at 1 and 2 mg/ml initial protein concentrations. The values of the fitted parameters are shown in Table 4. The calculated values of δ included in this table demonstrate that the external film resistance is in fact dominant at 0.2 mg/ml initial concentration while intraparticle transport becomes dominant when $C_0 \geq 1$ mg/ml.

The k_f values obtained in this study are consistent with values typically found for proteins in agitated vessels, as well as with the values predicted from engineering correlations for mass transfer to small particles [23,33]. As expected, these values become smaller for the larger proteins, as a result of the smaller solution diffusivity. The D_s values decrease with protein size much more dramatically, as can also be expected. However, the fitted D_s values

Table 4
Kinetic parameters obtained from the homogeneous diffusion model at different initial protein concentrations in 50 m*M* Tris–HCl buffer

Protein	k_f (10^{-3} cm/s)	D_s (10^{-9} cm^2/s)		$D_e C_0/D_s q_m$		$\delta = k_f r_p C_0/5 D_s q_m$	
		1 mg/ml	2 mg/ml	1 mg/ml	2 mg/ml	0.2 mg/ml	1 mg/ml
Lactalbumin	2.1	6.0	8.0	0.019	0.028	0.27	1.6
Ovalbumin	1.4	5.0	7.7	0.013	0.017	0.23	1.4
BSA[a]	1.0	2.4	2.4	0.034	0.068	0.53	2.6
Conalbumin	1.2	3.5	4.5	0.028	0.015	0.27	1.5
IgG	0.75	1.0	1.1	0.011	0.015	0.89	4.5

[a] From Ref. [24].

appear to increase somewhat as the initial protein concentration is increased from 1 to 2 mg/ml. For other ion-exchange media, intraparticle diffusion of proteins has been shown to be consistent with a driving force written in terms of the chemical potential gradient [22,34]. In this case, a certain concentration dependence of the effective diffusivity D_s could be expected [35]. Another explanation for these trends could be thought to be the existence of a parallel transport mechanism with a driving force expressed in terms of the fluid phase concentration. This would correspond to protein molecules diffusing within the particle without interaction with the electrostatic potential field at the pore wall. However, as shown by the chromatography results in Section 3.2, without binding these proteins access only a small fraction of the particle volume while the ratio D_e/D_0 is very small. We can estimate the relative importance of this potential contribution to the mass transfer flux, by considering the ratio $D_e C_0/D_s q_m$ [30]. As seen in Table 4, this ratio, representing the relative rates of pore and adsorbed-phase diffusion, has rather small values indicating that at these concentrations the contribution to the overall mass flux of the diffusion of protein molecules present within the particle but unadsorbed is very small.

An alternative approach to illustrate this effect is to fit the experimental uptake rate data with the so-called shrinking core model [30] using an apparent pore diffusivity $\tilde{D}_e$ as a fitting parameter and the previously determined values of k_f. This model assumes a rectangular isotherm, which is a good approximation for our experimental system. Typical results are shown in Fig. 6 for ovalbumin. The resulting apparent pore diffusivities normalized with respect to the free solution diffusivities are shown in Fig. 7. As seen in Fig. 6, the shrinking core model does not provide a good fit of the uptake curves at the higher initial concentrations. At 0.2 mg/ml the fit is better. However, it should be noted that with the shrinking core model, only a minimum value of $\tilde{D}_e$ can be determined at this initial concentration, since higher values would provide an equally good fit. As is shown in Fig. 7, the diffusivities derived from this model depend strongly on concentration and, in many cases, are several times greater than the free solution diffusivities, which is inconsistent with the underlying assumption of diffusion in a macroporous medium. By comparison, the diffusivities D_s obtained from the homogeneous diffusion model are much smaller than the corresponding free solution diffusivities, as could be expected for diffusion in a

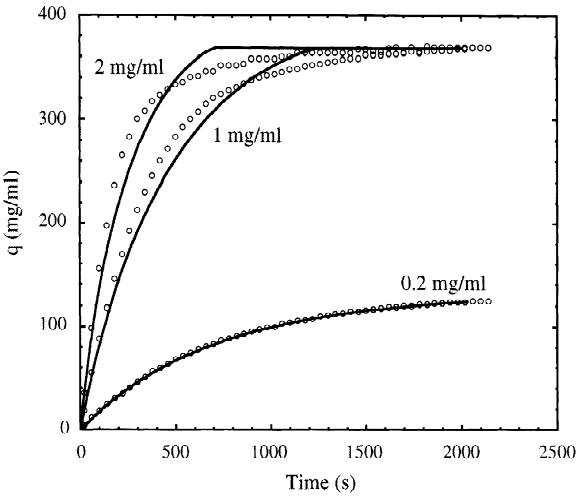

Fig. 6. Batch uptake curves for ovalbumin fitted with the shrinking core model.

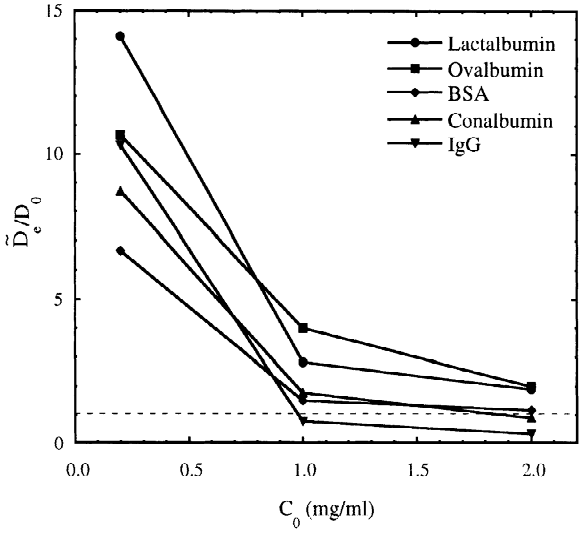

Fig. 7. Ratio of apparent pore diffusivities and free solution diffusivity determined from the shrinking core model fit of the experimental uptake rate data.

gel-medium [36]. Nevertheless, the high uptake rates observed experimentally for this material are still predicted by this model since the rate of diffusion is dependent on the product of D_s and the adsorption capacity, which is very high. Although not physically meaningful, the apparent pore diffusivity values shown in Fig. 7 still provide a measure of the enhancement of mass transfer rates resulting from favorable partitioning of these proteins in the particles [11,23]. These values can be compared directly to effective pore diffusivities determined for macroporous media where intraparticle transport is actually limited by diffusion in large, liquid-filled pores.

When comparing the D_s values obtained for the different proteins in BRX-Q, it is interesting to note that although the diffusivity generally decreases with molecular mass, the trend is not completely consistent with that of the free solution diffusivities. In particular, there is a much more pronounced effect of protein size. Moreover, conalbumin appears to have a somewhat larger diffusivity than BSA in spite of its larger size. The reasons for this behavior are not known. However, it is likely that diffusional transport in BRX-Q is affected by a complex set of factors including not just molecular size but also the net charge, the charge distribution, and the shape of the diffusing molecules. Since in BRX-Q transport occurs through a small-pore gel network, the adsorbed proteins diffuse while interacting strongly with the charged functional groups attached to the polymeric backbone. For these conditions, a dependence of diffusivity on this complex set of factors can be expected. On the other hand, the simple homogeneous diffusion model appears to capture the most important trends and permits a prediction of the column behavior of this adsorbent as previously demonstrated [18,25].

Lastly, the adsorption kinetics of ferritin was not investigated due to the very low capacity of the adsorbent for this protein. It is likely that the uptake of ferritin would be dominated by binding near the surface of the particle.

4. Conclusions

We have studied the equilibrium uptake, SEC behavior, and adsorption kinetics of several different model proteins with molecular masses in the range 15 000 to 450 000 on BRX-Q, an acrylamido-based anion-exchanger. This material is composed of dense polymer aggregates interspersed in a gel-like phase yielding a material that can withstand high flow-rates in packed columns but which also has a very high protein adsorption capacity. At a high salt concentration, when the electrostatic interaction responsible for binding is shielded, BRX-Q nearly completely excludes neutral macromolecules and large proteins, such as BSA. Smaller proteins, however, such as lactalbumin, are able to gain access to a small but significant fraction of the intraparticle volume. At a low salt concentration, the situation is completely different. In this case, the adsorption capacity for proteins as large as IgG is very high as a result of the favorable interaction with the charged functional groups in the media. Adsorption rates are also very rapid for these conditions. In fact, when the driving force for intraparticle diffusion is expressed as the concentration gradient in the fluid phase, diffusion coefficients several times greater than the free solution diffusivity are required to fit the data. A homogeneous diffusion model was found to be more consistent with the experimental uptake rate data predicting the experimentally observed trends with respect to protein concentration. Although the corre-

sponding diffusivity values are small and decline rapidly as the protein size is increased, high mass transfer rates are predicted because of the very favorable partitioning of these proteins on BRX-Q. From a practical viewpoint, the high adsorption capacity and rapid rates can be predicted to translate in high dynamic binding capacities that are generally desirable for capture applications.

5. Nomenclature

a	axial dispersion contribution to reduced HETP
b	adsorption isotherm parameter (ml/mg)
C	protein concentration in solution (mg/ml)
C_0	initial protein concentration in solution (mg/ml)
C_i	protein concentration in solution at particle-fluid interface (mg/ml)
d_p	particle diameter (cm)
D_0	free solution diffusivity (cm^2/s)
D_s	effective diffusivity based on homogeneous diffusion model (cm^2/s)
D_e	effective pore diffusivity (cm^2/s)
$\tilde{D}_e$	apparent pore diffusivity based on shrinking core model (cm^2/s)
k_f	external film mass transfer coefficient (cm/s)
k'	retention factor ($=(1-\varepsilon_b)K_D/\varepsilon_b$)
K_D	distribution coefficient
q	protein concentration in particle (mg/ml)
q_m	maximum adsorption capacity (mg/ml)
$\bar{q}$	average concentration in particle (mg/ml)
r	particle radial coordinate (cm)
r_p	particle radius (cm)
Sh	Sherwood number ($=k_f d_p/D_0$)
t	time (s)
v	mobile phase velocity (cm/s)
v'	reduced velocity ($=vd_p/D_0$)
V	solution volume (ml)
V_c	column volume (ml)
V_e	elution volume (ml)
V_M	volume of adsorbent particles (ml)
δ	parameter defined by Eq. (5)
ε_b	extraparticle void fraction

Acknowledgements

This research was supported by Bio-Rad Laboratories Inc., and NSF Grant No. CTS-0079334.

References

[1] E. Karlsson, L. Ryden, J. Brewer, in: J. Janson, L. Ryden (Eds.), Protein Purification, 2nd ed, Wiley–VCH, New York, 1998, Section 4.
[2] S. Yamamoto, K. Nakanishi, R. Matsuno, Ion Exchange Chromatography of Proteins, Marcel Dekker, New York, 1988.
[3] K. Miyabe, G. Guiochon, Biotechnol. Prog. 15 (1999) 740.
[4] R.K. Lewus, F.H. Altan, G. Carta, Ind. Eng. Chem. Res. 37 (1998) 1079.
[5] H. Guan-Sajonz, P. Sajonz, G. Zhong, G. Guiochon, Biotechnol. Prog. 12 (1996) 380.
[6] J.R. Conder, B.O. Hayek, Biochem. Eng. J. 6 (2000) 215.
[7] K. Miyabe, G. Guiochon, J. Chromatogr. A 866 (2000) 147.
[8] C. Chang, A.M. Lenhoff, J. Chromatogr. A 827 (1998) 281.
[9] P. Sajonz, H. Guan-Sajonz, G. Zhong, G. Guiochon, Biotechnol. Prog. 13 (1997) 170.
[10] H. Yoshida, M. Yoshikawa, T. Kataoka, AIChE J. 40 (1994) 2034.
[11] L.E. Weaver, G. Carta, Biotechnol. Prog. 12 (1996) 342.
[12] D.D. Frey, E. Schweinheim, C. Horvath, Biotechnol. Prog. 9 (1993) 273.
[13] D. Farnan, D.D. Frey, C. Horvath, Biotechnol. Prog. 13 (1997) 429.
[14] M. McCoy, K. Kalghatgi, F.E. Regnier, N. Afeyan, J. Chromatogr. A 743 (1996) 221.
[15] G.F. Bloomingburg, J.S. Bauer, G. Carta, C.H. Byers, Ind. Eng. Chem. Res. 30 (1991) 1061.
[16] E.M. Johnson, D.A. Berk, R.K. Jain, W.M. Deen, Biophys. J. 68 (1995) 1561.
[17] G.F. Bloomingburg, G. Carta, Chem. Eng. J. 55 (1994) B19.
[18] A.K. Hunter, G. Carta, J. Chromatogr. A 930 (2001) 79.
[19] G.L. Skidmore, B.J. Horstmann, H.A. Chase, J. Chromatogr. 498 (1990) 113.
[20] G. Garke, R. Hartmann, N. Papamichael, W.-D. Deckwer, F.B. Anspach, Sep. Sci. Technol. 34 (1999) 2521.
[21] A. Johnston, M.T.W. Hearn, J. Chromatogr. 557 (1991) 335.
[22] R.K. Lewus, G. Carta, AIChE J. 45 (1999) 512.
[23] M.A. Fernandez, G. Carta, J. Chromatogr. A 746 (1996) 169.
[24] A.K. Hunter, G. Carta, J. Chromatogr. A 897 (2000) 65.
[25] A.K. Hunter, G. Carta, J. Chromatogr. A 897 (2000) 81.
[26] P.G. Righetti, T. Caravaggio, J. Chromatogr. 127 (1976) 1.
[27] M.T. Tyn, T.W. Gusek, Biotechnol. Bioeng. 35 (1990) 327.

[28] M.E. Young, P.A. Carroad, R.L. Bell, Biotechnol. Bioeng. 22 (1980) 947.
[29] D. Farnan, D.D. Frey, C. Horvath, Biotechnol. Prog. 13 (1997) 319.
[30] M.D. LeVan, G. Carta, C.M. Yon, in: D.W. Green (Ed.), Perry's Chemical Engineers' Handbook, 7th ed, McGraw-Hill, New York, 1997, Section 16.
[31] F. Helfferich, Ion Exchange, McGraw-Hill, New York, 1962.
[32] M.S. Saunders, J.B. Vierow, G. Carta, AIChE J. 35 (1989) 53.
[33] P.M. Armenante, D.J. Kirwan, Chem. Eng. Sci. 44 (1989) 2781.
[34] J.A. Wesselingh, J.C. Bosma, AIChE J. 47 (2001) 1571.
[35] J.A. Wesselingh, R. Krishna, Mass Transfer in Multicomponent Mixtures, Delft University Press, Delft, The Netherlands, 2000.
[36] R.J. Phillips, W.M. Deen, J.F. Brady, AIChE J. 35 (1989) 1761.